Resolution enhancement in extended depth of field for volumetric two-photon microscopy

HONGSEN HE,[1] CIHANG KONG,[1,3] KA YAN CHAN,[1] W. L. SO,[2] HIU KA FOK,[2] YU-XUAN REN,[1] CORA S. W. LAI,[2] KEVIN K.TSIA,[1] AND KENNETH K. Y. WONG[1,*]

[1] *Department of Electrical and Electronic Engineering, The University of Hong Kong, Pokfulam Road, Hong Kong, China*
[2] *School of Biomedical Science, The University of Hong Kong, Pokfulam Road, Hong Kong, China*
[3] *Biomolecular Photonics, Department of Physics, University of Bielefeld, Universitätsstr, 25, 33615 Bielefeld, Germany*
**Corresponding author: kywong@eee.hku.hk*

Received XX Month XXXX; revised XX Month, XXXX; accepted XX Month XXXX; posted XX Month XXXX (Doc. ID XXXXX); published XX Month XXXX

The resolution enhancement over the extended depth of field (DOF) in the volumetric two-photon microscopy (TPM) is demonstrated by utilizing multiple orders of Bessel beam. Here, the conventional method of switching laser modes (SLAM) in 2D is introduced to 3D, denoted as the volumetric SLAM (V-SLAM). The equivalent scanning beam in the TPM is a thin needle-like beam, which is generated from the subtraction between the needle-like 0th-order and the straw-like 1st-order Bessel beam. Compared with the 0th-order Bessel beam, the lateral resolution of the V-SLAM is increased by 28.6% and maintains over the axial depth of 56 μm. The V-SLAM performance is evaluated by employing fluorescent beads and a mouse brain slice. The V-SLAM approach provides a promising solution to improve the lateral resolutions for fast volumetric imaging on sparsely distributed samples.

http://dx.doi.org/10.1364/OL.99.099999

Two-photon microscopy (TPM) with extended depth of field (DOF) has been investigated recently and applied in the study of neuroscience owing to its fast acquisition speed [1-3]. The extended DOF is usually created by spreading the focal spot in the axial direction, resulting in less scanning times to probe the entire volume of the sparsely distributed sample with a certain thickness. Nondiffractive beams, such as the needle-like Bessel beam [4, 5] and the curved Airy beam [6, 7], are generally utilized in the volumetric TPM as the excitation light due to the fact that they offer the constant transverse resolution at all depths of the volumetric sample [2]. However, the compromise of the extended DOF is that the lateral resolution is worse than the conventional TPM using the tightly-focused Gaussian beam. Moreover, the longer the nondiffractive beam, the worse the lateral resolution obtained [5]. Therefore, an approach to increase the lateral resolution over the extended DOF is demanded.

The concept of switching laser modes (SLAM) was first presented by Dehez *et al.* in 2013 to enhance resolution and contrast in laser scanning microscopy [8]. The SLAM method is based on the image subtraction obtained with the bright and dark mode, and exploits the smaller dimension of the dark spot. The advantages of the SLAM microscopy are its high temporal resolution compared with the single molecule imaging, and applicability to diverse imaging platforms and sample types [8]. Up to now, the SLAM methods are commonly applied in the 2D plane due to the tightly focused beam spot [9-14]. Korobchevskaya *et al.* also proposed the intensity-weighted subtraction (IWS) method for SLAM to minimize the oversubtraction and applied it for 3D resolution improvement [15]. In order to introduce the SLAM concept into the extended DOF microscopy in 3D, a pair of needle-like beams with bright and dark modes is required to conduct the subtraction for volumetric resolution enhancement.

Bessel beams are described by Bessel functions [16]. The azimuthal phase term existed in the electric field of the high-order Bessel beam contributes to a phase singularity along the center of the Bessel beam, creating a straw-like beam [17, 18]. The transverse shape over the beam length is an invariant doughnut profile, which is the same as the vortex beam, so that the high-order Bessel beam can be regarded as a dark mode and paired with the needle-like 0th-order Bessel beam (bright mode) to implement the subtraction based on the SLAM concept. Furthermore, the 0th-order and high-order Bessel beams have the equal axial depth when created by the same axicon, leading to a complete resolution enhancement and avoiding excessive subtraction over the whole beam length.

In this Letter, we demonstrate the application of the SLAM approach in the volumetric TPM to achieve the resolution enhancement in the extended DOF for volumetric imaging, denoted as the volumetric SLAM (V-SLAM). The needle-like 0th-order and straw-like 1st-order Bessel beams are regarded as the bright and dark modes, respectively. The axial resolution enhancement capability is evaluated by imaging fluorescent microspheres and a mouse brain slice.

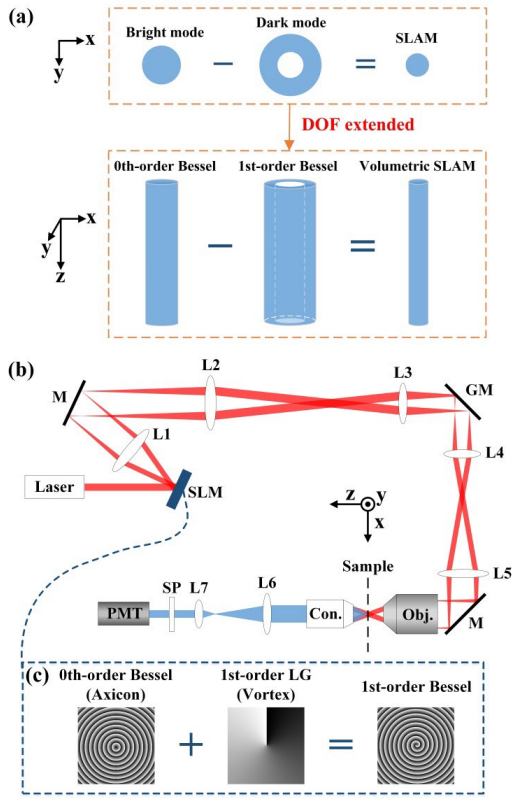

Fig. 1. (a) Principle of the conventional SLAM and the V-SLAM. (b) Experimental setup. (c) Phase masks loaded on the SLM and their superposition relationship. L, lens; SLM, spatial light modulator; GM, galvanometric mirror; M, mirror; Obj., objective; Con., condenser; SP, short-pass filter; PMT, photomultiplier tube.

Figure 1(a) shows the principle of the conventional SLAM and the V-SLAM. Based on the SLAM method in 2D, Bessel beams with multiple orders are utilized to extend the DOF of the microscopy such that the SLAM concept is introduced to 3D. Both the 0th-order and the 1st-order Bessel beam have axially elongated optical intensity distribution and maintain the same lateral beam size over an extended DOF [18]. The major difference between these two beams is that the 0th-order Bessel beam is a needle-like beam whose lateral shape is a solid spot, while the 1st-order Bessel beam is a straw-like beam whose lateral profile is a doughnut shape. The operation procedure of the V-SLAM is to sequentially illuminate the sample using the 0th-order and the 1st-order Bessel beam, then a subtraction is conducted between the two obtained images. The subtraction from the needle-like beam to the straw-like beam will generate a thinner needle-like beam, thus the equivalent lateral resolution is increased over the whole extended DOF.

Figure 1(b) shows the experimental setup of the resolution-enhanced volumetric TPM. A customized femtosecond mode-locked fiber laser served as the excitation light with the center wavelength of 1065 nm. A spatial light modulator (SLM, Holoeye, PLUTO) was used to load the phase masks of different Bessel beams. The diameter of the incident beam on the SLM screen was 4 mm. A lens (L1, focus length f_1 = 150 mm) after the SLM transformed the image of the Bessel beam into an annulus of light. L2 (f_2 = 250 mm) and L3 (f_3 = 125 mm) acted as a telescope to reduce the diameter of the annulus of light, so that it can match the working area of the 2D galvanometric mirror (GM, Cambridge Technology, 6220H). The other telescope consisted of L4 (f_4 = 80 mm) and L5 (f_5 = 150 mm) was used to expand the beam to illuminate the back aperture of a high numerical aperture (NA) water-immersion objective (Obj., 60×, 1.2 NA, UPlanSApo, Olympus). A condenser (Con., 1.4 NA) collected the stimulated fluorescent signal followed by a telescope (L6 and L7, f_6 = 100 mm and f_7 = 25.4 mm) to focus the signal into the photomultiplier tube (PMT, Hamamatsu H10723-20). The residual excitation beam around 1065 nm was filtered out by two short-pass (SP, BSP01-785R-25) filters before the PMT.

To generate different Bessel beams, the phase of excitation beam is required to be modified by the SLM. The electric field of the Bessel beam in the cylindrical coordinate can be written as [17]

$$E_l(r,\varphi,z) = E_0 \exp(ik_z z) J_l(k_r r) \exp(il\varphi), \quad (1)$$

where r and φ are the radial and azimuthal coordinates in the transverse plane, respectively. E_0 is the initial electric field intensity, l is the order of the Bessel beam, J_l is the lth-order Bessel function, and k_z and k_r are the longitudinal and radial wave-vector in the free space, respectively. According to Equation (1), the azimuthal phase term $\exp(il\varphi)$ will take effect when $l \geq 1$, which contributes to the generation of a phase singularity in the center of the Bessel beam along the axial direction. Thus the lateral profile of the high-order Bessel beam is the same as the vortex beam with orbital angular momentum (OAM). Based on this principle, the high-order Bessel beam can be generated by illuminating the OAM beam through the axicon [18]. Fortunately, the SLM here acts as an integrated phase modulator, which can not only play the part of the axicon but also offer the spiral phase of the OAM beam. The phase distribution of the 0th-order Bessel beam consists of concentric circles [Fig. 1(c)]. By adjusting the interval of the rings, the cone angle of the axicon can be varied, resulting in different axial depths of Bessel beam. The 0th-order Bessel beam will be generated after the fundamental Gaussian beam incident on the SLM screen. For high-order Bessel beams, an azimuthal phase mask is uploaded into the SLM and superimposed with the concentric phase mask, then a spiral concentric phase distribution will be obtained [Fig. 1(c)]. The order of the Bessel beam is determined by the order of the OAM beam. Specifically, when the azimuthal phase corresponds to the 1st-order Laguerre-Gaussian (LG) beam, the spiral concentric phase mask is corresponding to the 1st-order Bessel beam.

To illustrate the point spread function (PSF) of the Bessel beam in the TPM, a single fluorescent microsphere (diameter 100 nm, F8800, Life Technologies Ltd.) was scanned in x-y plane. Figure 2(a) and (b) show the lateral profiles of the 0th-order Bessel beam (solid spot) and the 1st-order Bessel beam (doughnut shape), respectively. Obviously, the hollow size of the doughnut beam is smaller than the solid spot. According to the SLAM concept, the 0th-order and 1st-order Bessel beam can be regarded as the bright and dark mode, respectively. The subtracted PSF is given as [8]

$$PSF_{\mathrm{SLAM}} = PSF_{\mathrm{bright}} - g \cdot PSF_{\mathrm{dark}}, \quad (2)$$

where g is the subtraction coefficient. A higher value of g contributes to a higher lateral resolution, but simultaneously it also introduces large negative values around the object, which will deteriorate the imaging quality. The subtraction coefficient is commonly restricted to $0.5 \leq g \leq 1$. g = 0.5 is set during our experiments to avoid excessive subtraction. Figure 2(c) shows the resolution-enhanced image from the subtraction of Figure 2(a) to

(b). Evidently, the spot size in Figure 2(c) is smaller than that in Figure 2(a). In Figure 2(d), the intensities of the three beams are all normalized in order to compare their full width at half-maximum (FWHM). The FWHMs of the 0th-order Bessel beam and the subtracted Bessel beam are 700 and 500 nm, respectively. Therefore, the lateral resolution is increased by 28.6% after the subtraction. As aforementioned, the resolution can be further improved by choosing a larger value of g, which should depend on specific applications while avoiding image deterioration.

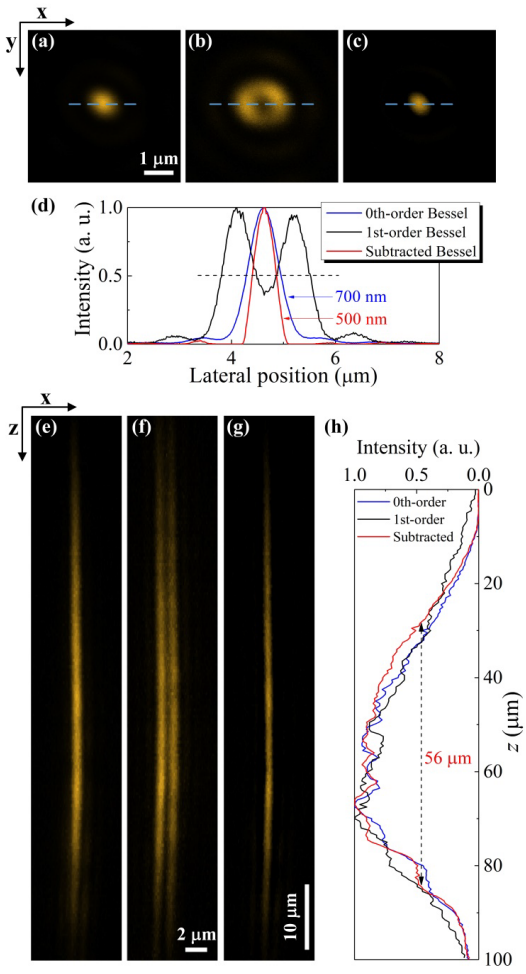

Fig. 2. Lateral profile of the 0th-order Bessel beam (a) and the 1st-order Bessel beam (b). (c) Subtracted image from (a) and (b). (d) PSFs of the 0th-order Bessel beam, 1st-order Bessel beam and subtracted Bessel beam in x-y plane. (e-g) Corresponding axial intensity distribution in x-z plane of (a-c). (h) Axial beam profiles correspond to (e-g).

To obtain the optical intensity distributions of the Bessel beams in the axial direction of the TPM, the fluorescent microsphere is moved along z-axis with a step of 0.5 μm. The 1st-order Bessel beam [Fig. 2(f)] maintains the doughnut profile along the z-axis, and the extended DOF is equal to the 0th-order Bessel beam [Fig. 2(e)]. Thus, it is a good match for the pair of Bessel beams to achieve the V-SLAM. Figure 2(g) shows the subtracted image in x-z plane. After subtraction, a thinner needle-like beam is obtained while maintains the same axial depth, compared with the 0th-order Bessel beam. Thus, the lateral resolution is enhanced over the extended DOF. The axial FWHM of the subtracted Bessel beam is 56 μm, and the three beams have nearly equal axial widths [Fig. 2(h)]. The axial length of the Bessel beams can be further extended but simultaneously it will sacrifice the lateral resolution and the intensity of the fluorescent signal.

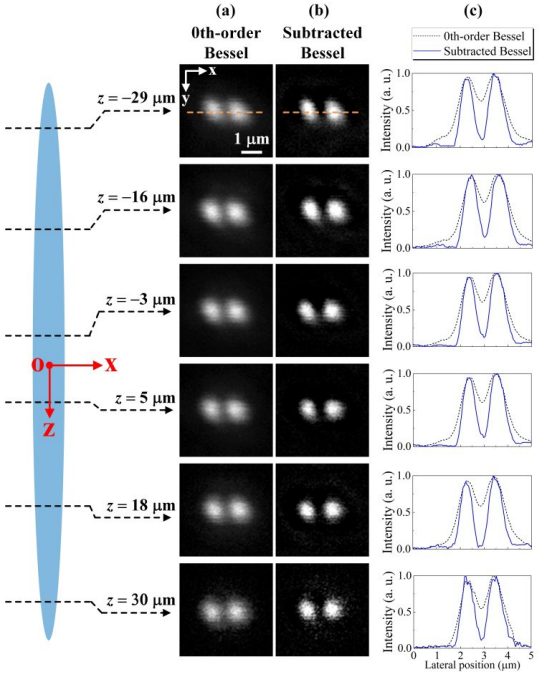

Fig. 3. 0th-order-Bessel-beam (a) and subtracted (b) images of two adjacent fluorescent microspheres scanned at six positions along the beam axis. (c) Corresponding intensity profile of the two beads.

The system performance of the V-SLAM is evaluated by imaging two adjacent fluorescent microspheres (diameter 1 μm, F8819, Life Technologies Ltd.) at different positions along the beam axis, as shown in Figure 3. The two beads were moved along the z-axis from $z = -29$ μm to $z = 30$ μm. $z = 0$ is set to be the center position along the axial direction of the Bessel beams. Six positions with nearly even intervals were scanned by the pair of Bessel beams, then subtractions were conducted at each position. In contrast to the image scanned by the 0th-order Bessel beam [Fig. 3(a)], the subtracted image [Fig. 3(b)] shows clearer profiles of the two beads. Meanwhile, as shown in Figure 3(c), dip from the subtracted image between the two intensity peaks is much deeper than that from the original image, which also indicates a good resolution improvement. Furthermore, for all the six positions, both the subtracted images and graphs demonstrate consistent resolution-enhanced performance, illustrating that the V-SLAM approach is capable to increase the lateral resolution over the whole extended DOF.

To demonstrate the V-SLAM applicability on biological tissues in the TPM, a 50-μm-thick mouse brain tissue sandwiched by two glass slides was prepared for imaging. The mouse expresses the yellow fluorescent protein (YFP) in a subset of motor and sensory neurons (Thy1-YFP H-line). Layer-V pyramidal neurons in prefrontal cortex were imaged in this article. All experiments with these samples were approved and performed in accordance with institutional guidelines of the University of Hong Kong.

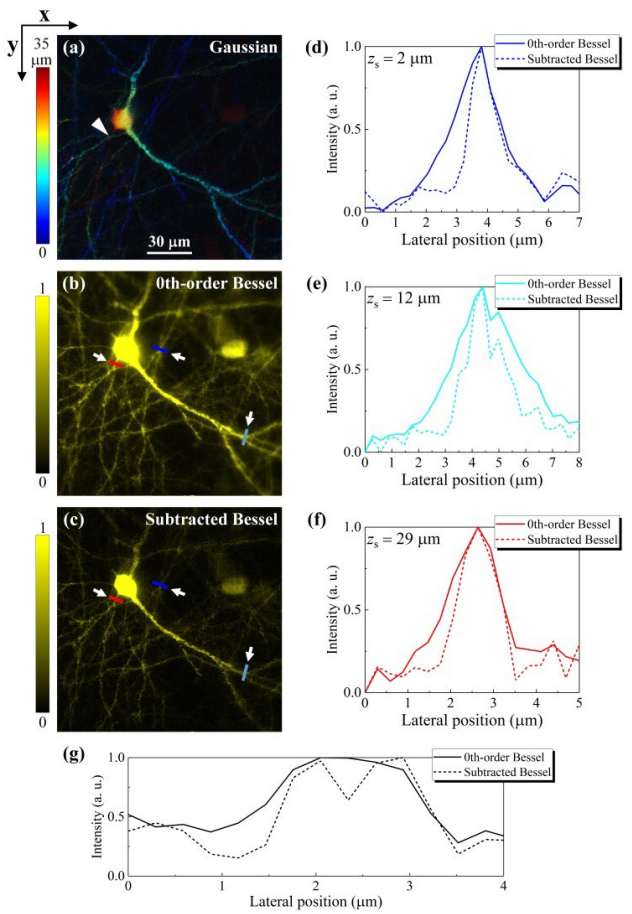

Fig. 4. (a) Projected image of the Gaussian-scanned stacks of the mouse brain slice. (b) 0th-order-Bessel-beam scanned image. Frame rate: ~0.37 Hz for 512 x 512 pixels. (c) Subtracted image. Brightness of (b) and (c): times a factor of 8 to demonstrate all the neurons clearly. (d-f) Comparison of lateral intensity profiles of mouse brain neurons at different depths (z_s = 2, 12 and 29 μm) between (b) and (c). The three positions are pointed by the white arrows both in (b) and (c). (g) Distinction of two neurons at a denser area of the sample after subtraction. The neuron position is pointed in (a).

Firstly, the mouse brain was scanned layer by layer by the Gaussian beam with a step of 0.5 μm along *z*-axis. The neurons were observed to distribute within the depth of 35 μm inside the section. The axial position of different layers is color-coded in Figure 4(a). To protect the brain tissue against photobleaching, the average power of the Gaussian beam after the objective was set to be 19 mW, which results in a slightly lower intensity of the fluorescent signal. Then under the post-objective power of 120 mW, and the mouse brain was volumetrically scanned by the 0th-order and the 1st-order Bessel beam sequentially. Comparing Figure 4(b) and (c), the contrast in the subtracted image is enhanced while the details are all maintained. The contrast enhancement performance is an intrinsic property of the SLAM method owing to the fact that the negative values beyond the edges of the bright beam are all set to zero [8]. The quantitative demonstrations for the resolution enhancement of the V-SLAM at different depths with the range of 27 μm are shown in Figure 4(d-f). z_s = 0 denotes the beginning edge of the neuron distributions in the sample. At z_s = 2, 12 and 29 μm, the neuron widths in the subtracted image are all narrower than those in the original image, which is well consistent with the concept of the V-SLAM approach. The slightly asymmetric subtraction in Figure 4 (d) and (f) is owing to unhomogeneous intensity distribution of the 1st-order Bessel beam. Figure 4(g) shows the V-SLAM performance for distinguishing adjacent neurons. After subtraction, two neuron peaks are shown compared with the original image with an indistinguishable peak.

In conclusion, we have demonstrated the resolution enhancement over the extended DOF in the volumetric TPM based on the V-SLAM approach. The 0th-order and the 1st-order Bessel beam serve as the bright and dark mode, respectively. The subtraction is completely conducted due to the equal axial depth of the pair of Bessel beams. Bessel beams of different orders are switchable on the SLM, resulting in an easy operation of the V-SLAM approach. Compared with the 0th-order Bessel beam, the lateral resolution of the V-SLAM is increased by 28.6% and maintains over the axial depth of 56 μm. The V-SLAM approach provides a promising solution to improve the lateral resolutions for fast volumetric imaging on sparse samples.

Funding. Research Grants Council, University Grants Committee (HKU 17200219, HKU 17209018, E-HKU701/17HKU C7047-16G, CityU T42-103/16-N); National Natural Science Foundation of China (61631166003, 61675081, N_HKU712/16).

Disclosures. The authors declare no conflicts of interest.

References

1. R. Lu, W. Sun, Y. Liang, A. Kerlin, J. Bierfeld, J. D. Seelig, D. E. Wilson, B. Scholl, B. Mohar, and M. Tanimoto, Nat. Neurosci. **20**, 620 (2017).
2. G. Thériault, Y. De Koninck, and N. McCarthy, Opt. Express **21**, 10095 (2013).
3. G. Thériault, M. Cottet, A. Castonguay, N. McCarthy, and Y. De Koninck, Front. Cell. Neurosci. **8**, 139 (2014).
4. B. Chen, X. Huang, D. Gou, J. Zeng, G. Chen, M. Pang, Y. Hu, Z. Zhao, Y. Zhang, and Z. Zhou, Biomed. Opt. Express **9**, 1992 (2018).
5. C. Rodriguez, Y. Liang, R. Lu, and N. Ji, Opt. Lett. **43**, 1914 (2018).
6. X.-J. Tan, C. Kong, Y.-X. Ren, C. S. Lai, K. K. Tsia, and K. K. Wong, Opt. Lett. **44**, 391 (2019).
7. H. He, C. Kong, X.-J. Tan, K. Y. Chan, Y.-X. Ren, K. K. Tsia, and K. K. Wong, Opt. Lett. **44**, 5238 (2019).
8. H. Dehez, M. Piché, and Y. De Koninck, Opt. Express **21**, 15912 (2013).
9. L. Thibon, L. E. Lorenzo, M. Piché, and Y. De Koninck, Opt. Express **25**, 2162 (2017).
10. L. Thibon, M. Piché, and Y. De Koninck, Opt. Express **26**, 24881 (2018).
11. A. Gasecka, A. Daradich, H. Dehez, M. Piché, and D. Côté, Opt. Lett. **38**, 4510 (2013).
12. M. Yoshida, Y. Kozawa, and S. Sato, Opt. Lett. **44**, 883 (2019).
13. S. Segawa, Y. Kozawa, and S. Sato, Opt. Lett. **39**, 3118 (2014).
14. C. J. Sheppard, Optics letters **36**, 1386 (2011).
15. K. Korobchevskaya, C. Peres, Z. Li, A. Antipov, C. J. Sheppard, A. Diaspro, and P. Bianchini, Scientific reports **6**, 25816 (2016).
16. J. Durnin, J. Miceli Jr, and J. Eberly, Phys. Rev. Lett. **58**, 1499 (1987).
17. J. Arlt, and K. Dholakia, Opt. Commun. **177**, 297 (2000).
18. X. Wei, C. Liu, L. Niu, Z. Zhang, K. Wang, Z. Yang, and J. Liu, Appl. Optics **54**, 10641 (2015).

References with titles

1. R. Lu, W. Sun, Y. Liang, A. Kerlin, J. Bierfeld, J. D. Seelig, D. E. Wilson, B. Scholl, B. Mohar, and M. Tanimoto, "Video-rate volumetric functional imaging of the brain at synaptic resolution," Nat. Neurosci. **20**, 620 (2017).
2. G. Thériault, Y. De Koninck, and N. McCarthy, "Extended depth of field microscopy for rapid volumetric two-photon imaging," Opt. Express **21**, 10095-10104 (2013).
3. G. Thériault, M. Cottet, A. Castonguay, N. McCarthy, and Y. De Koninck, "Extended two-photon microscopy in live samples with Bessel beams: steadier focus, faster volume scans, and simpler stereoscopic imaging," Front. Cell. Neurosci. **8**, 139 (2014).
4. B. Chen, X. Huang, D. Gou, J. Zeng, G. Chen, M. Pang, Y. Hu, Z. Zhao, Y. Zhang, and Z. Zhou, "Rapid volumetric imaging with Bessel-Beam three-photon microscopy," Biomed. Opt. Express **9**, 1992-2000 (2018).
5. C. Rodriguez, Y. Liang, R. Lu, and N. Ji, "Three-photon fluorescence microscopy with an axially elongated Bessel focus," Opt. Lett. **43**, 1914-1917 (2018).
6. X.-J. Tan, C. Kong, Y.-X. Ren, C. S. Lai, K. K. Tsia, and K. K. Wong, "Volumetric two-photon microscopy with a non-diffracting Airy beam," Opt. Lett. **44**, 391-394 (2019).
7. H. He, C. Kong, X.-J. Tan, K. Y. Chan, Y.-X. Ren, K. K. Tsia, and K. K. Wong, "Depth-resolved volumetric two-photon microscopy based on dual Airy beam scanning," Opt. Lett. **44**, 5238-5241 (2019).
8. H. Dehez, M. Piché, and Y. De Koninck, "Resolution and contrast enhancement in laser scanning microscopy using dark beam imaging," Opt. Express **21**, 15912-15925 (2013).
9. L. Thibon, L. E. Lorenzo, M. Piché, and Y. De Koninck, "Resolution enhancement in confocal microscopy using Bessel-Gauss beams," Opt. Express **25**, 2162-2177 (2017).
10. L. Thibon, M. Piché, and Y. De Koninck, "Resolution enhancement in laser scanning microscopy with deconvolution switching laser modes (D-SLAM)," Opt. Express **26**, 24881-24903 (2018).
11. A. Gasecka, A. Daradich, H. Dehez, M. Piché, and D. Côté, "Resolution and contrast enhancement in coherent anti-Stokes Raman-scattering microscopy," Opt. Lett. **38**, 4510-4513 (2013).
12. M. Yoshida, Y. Kozawa, and S. Sato, "Subtraction imaging by the combination of higher-order vector beams for enhanced spatial resolution," Opt. Lett. **44**, 883-886 (2019).
13. S. Segawa, Y. Kozawa, and S. Sato, "Resolution enhancement of confocal microscopy by subtraction method with vector beams," Opt. Lett. **39**, 3118-3121 (2014).
14. C. J. Sheppard, "Binary phase filters with a maximally-flat response," Opt. Lett. **36**, 1386-1388 (2011).
15. K. Korobchevskaya, C. Peres, Z. Li, A. Antipov, C. J. Sheppard, A. Diaspro, and P. Bianchini, "Intensity weighted subtraction microscopy approach for image contrast and resolution enhancement," Sci. Rep. **6**, 25816 (2016).
16. J. Durnin, J. Miceli Jr, and J. Eberly, "Diffraction-free beams," Phys. Rev. Lett. **58**, 1499 (1987).
17. J. Arlt, and K. Dholakia, "Generation of high-order Bessel beams by use of an axicon," Opt. Commun. **177**, 297-301 (2000).
18. X. Wei, C. Liu, L. Niu, Z. Zhang, K. Wang, Z. Yang, and J. Liu, "Generation of arbitrary order Bessel beams via 3D printed axicons at the terahertz frequency range," Appl. Optics **54**, 10641-10649 (2015).